Parametric Analysis of Waste Heat Driven Vapor Absorption System for Space Conditioning in Automobiles

Dr. Tauseef Aized[*1], Muhammad Noman[2]

1. *Mechanical Engineering Department University of Engineering and Technology, Lahore*
2. *Muhammad Nawaz Sharif University of Engineering and Technology, Multan*

∗ **Corresponding Author:** Email: tauseef.aized@uet.edu.pk

Abstract

In this work, a single effect ammonia water-based waste heat driven vapor absorption system was investigated and conceptualized. Exhaust gases from diesel engine have been utilized as a heat source to run the vapor absorption system for space conditioning in automobiles. Daewoo bus, model BH116 was chosen for this analysis. The cooling load of the bus was calculated based on the local weather condition of Lahore for the month of June. Heat balance method technique was implemented to calculate the cooling load of the bus. The cooling load calculated was 29.886 kW. The displacement of the engine was 11051 cc. A thermodynamic model was established using MATLAB software program and the system performance was analyzed over a range of operating conditions. It was studied that the engine was capable to generate that much heat which could be utilized to produce the required cooling inside the bus.

Key Words: Waste heat, Vapor absorption system, Exhaust gases, Ammonia-Water

Nomenclature		Subscripts	
Symbols		A	Air
Q	Heat input, kJ	Dir	Direct
M	Metabolic load, W	Dif	Diffused
A	Area, m^2	Ref	Reflected
W	Average width of passengers, m	Amb	Ambient
h	Average height of passengers, m	Exh	Exhaust
$_i$	Radiation intensity, W/m^2	Eng	Engine
τ	Transmittivity	Ven	Ventilation
S	Surface area, m^2	Ac	Air conditioning
θ	Solar altitude angle	Du	DuBois
U	Overall heat transfer coefficient, $W/(m^2K)$	Met	Metabolic
T	Temperature, K	I	Inside
R	Resistivity, $(m^2K)/W$	O	Outside
H	Heat transfer coefficient, $W/(m^2K)$	F	Fuel
Λ	Thickness of the wall, m		
K	Conduction heat transfer coefficient, $W/(m^2K)$		
v	Specific Volume (m^3/kg)		
V	Velocity of air		
$\dot{m}$	Mass flow rate		
X	Humidity ratio		
x	Ammonia concertation		
$\dot{Q}$	Heat load per unit time, W		
W	Average width of passengers		

1. Introduction

Energy efficient systems have become a key topic of discussion for the reduction of natural resource utilization [1]. Exhaust emissions from the burning of fossil fuel like coal, furnace oil, diesel, petrol, liquid petroleum gas (LPG) and liquefied natural gas (LNG) in factories and transportation sector including trucks, buses, cars and electricity production from power plants has degraded the quality of environment [2]. The transport sector is the major drivers of oil consumption, about half of the worldwide oil is utilized in the transportation sector [3]. Performance of internal combustion is subjected to continuous optimization to increase efficiency.

Use of air conditioning system in the automobiles has become an essence of modern life. Conventionally, to run these air conditioning systems the compressor is coupled with the engine. A huge amount of energy is utilized to run these air conditioning systems in the vehicles. One-third of the fuel energy is wasted through the exhaust gases. These exhaust gases have a huge amount of energy and are recyclable. One of the methods to utilize this waste heat is to operate vapor absorption systems which is an effective substitute of conventional vapor compression cycle which utilize high-grade energy [1, 4].

Yuan et al. [5] performed experimentation to meet the onboard ship refrigeration requirement through exhaust heat driven vapor absorption refrigeration system. Considering the adverse effect on the ship ternary ammonia–water-lithium bromide mixture is used as a working fluid in the vapor absorption system. A temperature of -15 ℃ was achieved through this waste heat driven system. Ouadha & El-gotni [6] examined the feasibility of operation of ammonia water based waste heat driven vapor absorption system using engine exhaust heat. It was observed that the coefficient of performance (COP) of the cycle increases with a decrease in absorber and condenser temperature and an increase of evaporator temperature. Rêgo et al. [7] experimentally analyzed vapor absorption by connecting the generator with the exhaust of diesel engine. The performance of the cycle was evaluated by varying engine speed, torque and key temperature in the absorption cycle. The results showed that the performance of the vapor absorption cycle enhanced by control of input heat to the generator. Asadi et al. [8] conducted an analysis on solar heat driven single effect vapor absorption system to produce cooling of 10 kW. Performance of vapor absorption system was observed using various collector types including flat plate collector, evacuated tube collector, compound parabolic and parabolic trough collector. It was concluded that solar evacuated tube collector provides the most economical solution with least collector area. Shiue [9] performed an experimental study of lithium bromide/water-based waste heat driven vapor absorption system. The plant was operated using heat from municipal solid waste incineration plant. The study concluded that the COP of the system increases with the decrease of condenser and absorber and an increase of evaporator temperature. Buonomano et al. [10] simulated solar heat driven vapor absorption system for space conditioning inside the buildings. Simulation was performed by writing codes in MATLAB. Monthly based solar irradiation data was used to compute the performance of the system. Shi et al. [11] performed an experimental study by driving a double effect vapor absorption cycle with multi-heat sources. Two heat sources were used to run lithium-bromide/water-based vapor absorption cycle. It was observed that COP of this double effect vapor absorption cycle is 20% more than single effect vapor absorption cycle. Staedter & Garimella [12] developed a small-scale ammonia water-based vapor absorption system to produce 7 W cooling effect. The vapor absorption cycle was operated using a microchannel heat exchanger. The experimental study achieved the COP of 0.51. Staedter & Garimella [13] developed a gas-coupled vapor absorption system to produce small scale cooling. The experiment concluded the feasibility of gas-coupled vapor absorption system for small scale cooling. M. Wang et al. [14] conceptualized high-temperature exhaust heat driven double effect vapor absorption system for refrigeration purpose of onboard ship refrigeration. Non-volatile ionic liquids are utilized as an absorbent in the cycle. The study concluded that by this waste heat driven cycle the CO2 emission could reduce up to 1633.5 tons. Yousfi et al. [15] performed an experimental evaluation of diffusion-absorption chiller. The chiller has been tested by varying different parameters. COP of the system was observed to be 0.45 with a cooling capacity of 4.52 W. The study proposed heat from solar or exhaust of an engine to run the chiller. Aly et al. [16] developed an experimental setup to run the vapor absorption cycle on the exhaust from a diesel engine. The cycle was observed at different engine load. The torque and flow rate of exhaust was varied to observe the performance of the cycle. COP of the vapor absorption cycle was observed to be 0.10. Du et al. [17] conducted an experimental study on the ammonia water-based exhaust heat driven vapor absorption. The exhaust heat taken from the diesel engine was varied to optimize the performance of the absorption cycle. The cycle gained maximum COP of 0.53 with a cooling capacity of 33.8kW. Ibrahim et al. [18] performed simulation of a solar heat driven vapor absorption system by integrating it with an absorption energy storage. The lithium-bromide/ water-based vapor absorption system provides cooling as well as storing of energy in the absorption energy storage during the hours of solar radiation. The simulation results showed that the system could produce cooling of 20 kW. Salmi et al. [19] presented a model of vapor absorption system driven by the waste heat of a ship. The system performance is observed by varying generator and evaporator

temperature. Exhaust gas from the engine, scavenging air and jacket water were taken as a heat source. Shu et al. [20] performed an experimental study of compressor assisted vapor absorption cycle. The lithium-bromide/water-based vapor absorption system was attached with a Rankine cycle as a heat input source. Xu & Wang [21] simulated variable effect solar assisted vapor absorption chiller. Compound parabolic collector was used to observe the performance of the system. TRANSYS simulation program was chosen to evaluate the performance of the system. Xu & Wang [22] simulated a compound parabolic collector-based vapor absorption system. Single effect, double effect and multi-effect vapor absorption systems were optimized. Yang et al. [23] proposed number of methods to utilize waste heat organic Rankine cycles (ORC), absorption chillers, absorption heat pumps, absorption heat transformers, and mechanical heat pumps can utilize waste heat to produce electricity, heating and cooling effect. Palomba et al. [24] performed simulation to check the feasibility of two waste heat driven vapor absorption system for space conditioning for onboard application. The result of the calculation showed that it could save 1000 kg of fuel per year. Mumtaz et al. [25] performed experimentation on solar driven vapor absorption system. To obtain continuous cooling the absorption chiller was attached with the two-alternative storage unit containing chilled water and ice. Zisheng & Ruzhu [26] presented a multistep sorption cycle for space conditioning in fishing vessels. The study concluded that the cycle has the ability to produce 15.4 kW/m3. Shi et al. [27] presented a waste heat driven vapor absorption system for high temperature glide. The simulation result concluded that this design is 20% more efficient than the single effect absorption system. R. Z. Wang et al. [28] modelled a solar heat driven sorption system. Performance of absorption and adsorption system were observed using different working fluid including silica gel–water adsorption chiller, single/double effect LiBr–water absorption chiller. Brückner et al. [29] presented different waste heat driven technologies including the vapor absorption cycle. The economic analysis of each technology was also performed. Cao et al. [30] performed a simulation study of waste heat driven vapor absorption system for cooling in the shipboard application. The system was also compared with vapor compression cycle has electricity input-based COP of 9.4. Patel et al. [31] performed a thermos-economic optimization of organic Rankine cycle powered cascaded system. Dry organic working fluid was used to obtain power. The system achieved lower temperature cooling effectively. The evaluated time for payback period was found to be 4.5 years.

The focus of this study is to design a waste heat driven vapor absorption system for a transportation system. The idea of cooling load is achieved by calculating the cooling load of Daewoo BH116 bus using MATLAB software. Major components of waste heat driven vapor absorption system are modeled in detail using MATLAB software.

2. Mathematical Modelling

To get an idea of cooling to be produced, cooling load of a bus is calculated then an exhaust gas driven system is modeled to produce required cooling.

2.1 Cooling load calculation of bus

MATLAB software is used to calculate the cooling load of Daewoo bus model BH116. The total seating capacity of bus includes 49 seats for passengers and 1 seat for the driver. An overview of the bus can be seen from Fig. 1.

The cooling load of the bus was calculated using Heat balance method (HBM) technique. The cooling load calculation was based on the Lahore region. The climate of Pakistan is typically warm; the temperature rises to 48˚C in the month of June. The wind velocity is not constant. These conditions create an adverse impact on driver concentration. The cooling load has been calculated for a full day. The cooling load of vehicles reaches its peak at noon.

The heat gained by the vehicle was categorized into nine different types. If the sum of all these heat gains is positive, then the cabin will be heating up and if negative then the cabin will be cooling down. The correlation presented in this study can be readily used to model any other automobile

The mathematical model for the cooling load calculation can thus be abridged as

$$\dot{Q}_{Tot} = \dot{Q}_{Met} + \dot{Q}_{Dir} + \dot{Q}_{Dif} + \dot{Q}_{\mathrm{Re}f} + \dot{Q}_{Amb} + \dot{Q}_{Exh} + \dot{Q}_{Eng} + \dot{Q}_{Ven} + \dot{Q}_{Ac} \quad (1)$$

2.1.1 Metabolic Load

Due to the metabolic activities taking place inside the human body, continuous heat and humidity are produced. The heat gain from the human body is considered as a metabolic load.

The relationship for metabolic load calculation is given below.

$$\dot{Q}_{Met} = \sum_{Passenger} MA_{DU} \quad (2)$$

Where ADU is DuBois area, which was obtained from the following relationship.

$$A_{DU} = 0.202W^{0.425}h^{0.725} \quad (3)$$

The average height of passenger was taken as 5 feet 3 inch and average width was 1 foot 6 inch [32].

2.1.2 Radiation load

Solar radiation has a greater impact of heat gain in the cabin. According to ASHRAE the heat gain from solar radiation can be categorized into three types direct, diffused, and reflected heat loads.

Direct heat load is the load which is gained by direct solar radiations. Following relation was used to formulate the direct heating load.

$$\dot{Q}_{Dir} = \sum_{Surfaces} S\tau i_{Dir} \cos\theta \quad (4)$$

Diffuse radiation results due to the indirect radiations of the daylight on the surface. The heat gain by diffuse radiation was calculated using the following relation.

$$\dot{Q}_{Diff} = \sum_{Surfaces} S\tau i_{Diff} \quad (5)$$

Reflected radiation is referred to those radiations which get reflected after striking the road surface and strikes the vehicle body. It was calculated using the following relationship.

$$\dot{Q}_{ref} = \sum_{Surfaces} S\tau i_{ref} \quad (6)$$

2.1.3 Ambient load

Ambient load is created inside the cabin due to the circulation of ambient air inside the cabin. The load depends upon the temperature difference between the cabin air and the ambient air.

$$\dot{Q}_{amb} = \sum_{Surfaces} SU(T_s - T_i) \quad (7)$$

Where U can be computed from the following relation.

$$U = \frac{1}{R} \quad (8)$$

$$R = \frac{1}{h_o} + \frac{\lambda}{k} + \frac{1}{hi} \quad (9)$$

Where R is the net thermal resistance, ho and hi are the convection heat transfer coefficient, λ is the thickness of the body material and k is the conduction heat transfer coefficient.

$$h = 0.6 + 6.64\sqrt{V} \quad (10)$$

V is the velocity of air measured in m/s. The air inside the cabin is considered stationary and the outside air velocity is considered equal to the speed of the bus.

2.1.3.1 Exhaust load

Both conventional and hybrid vehicles have an internal combustion engine. Heat can transfer through the surface area of exhaust that is in touch with the cabin surface. The exhaust load was calculated using the following relation.

$$\dot{Q}_{Exh} = \sum_{Surfaces} S_{Exh}U(T_{Exh} - T_i) \quad (11)$$

Where U can be calculated using equation no 8. Texh was obtained using the following relation.

$$T_{EXH} = 0.138RPM - 17 \quad (12)$$

Where RPM is the revolution per minute of the engine.

2.1.4 Engine load

Same as exhaust load, the engine has a greater impact in increasing the cooling load. The heat from the engine transfers to the vehicle body by convection heat transfer.

$$\dot{Q}_{Eng} = \sum_{Surfaces} S_{Eng}U(T_{Eng} - T_i) \quad (13)$$

The engine temperature was measured using the following relation.

$$T_{Eng} = -2\times10^{-6}RPM^2 + 0.0355RPM + 77.5 \quad (14)$$

2.1.5 Ventilation load

Fresh air from outside of the vehicle is circulated in the cabin to keep the cabin air fresh. But this circulation causes load on the air conditioner because of the difference of outside air temperature to the cabin air temperature. The thermal heat gain by this fresh air was calculated by the following relation.

$$\dot{Q}_{Ven} = \dot{m}_{Ven}(e_o - e_i) \quad (15)$$

Where eo is the enthalpy of outside air and ei is the enthalpy of inside air which was measured by the following relation [33].

$$e = 1006T + (2.501\times10^6 + 1770T)x \quad (16)$$

2.2 Thermal analysis of vapor absorption cycle

Thermal analysis was performed by heat balance method. Heat balance was performed at each component of the cycle. The computations to check the performance waste heat driven vapor absorption cycle has done using MATLAB Software platform. Fig. 2 shows the Model of exhaust gas driven vapor absorption cycle. Summary of working parameters are given in Table 2.

2.2.1 Evaporator

At the evaporator, the coolant enters the evaporator enters from one side in the liquid form and exit in the gaseous form. The latent heat is absorbed in the evaporator. There was the 1˚C rise of temperature was considered.

$$Q_{evp} = (h_{11} - h_{10})m_{11} \quad (17)$$

2.2.2 Absorber

In the absorber, the working fluid enters the absorber and mixes with the weak solution. The heat from the absorber is emitted in the atmosphere. The heat loss by the absorber was calculated by the following relation.

$$Q_{abs} = m_{12}h_{12} + m_6h_6 - m_1h_1 \quad (18)$$

2.2.3 Generator

In the generator, heat is added from the exhaust gas coming from vehicle exhaust. The heat is transferred to the generator by a heat exchanger. The strong solution is entering the generator from one side and the weak solution is leaving the generator on the other side.

$$Q_{gen} = m_{13}h_{13} + m_4h_4 - m_3h_3 - m_{14}h_{14} \quad (19)$$

2.2.4 Pump

Pump delivers the strong solution from the absorber to the generator at an elevated pressure. Pump work was obtained using the following relation.

$$\dot{W}_p = (p_2 - p_1)v_2 \quad (20)$$

2.2.5 Condenser

In the condenser, ammonia gas enters the condenser from one side. The ammonia releases the latent heat and leaves in the liquid phase. The heat releases from the condenser by convection heat transfer and was obtained by using the following relation.

$$Q_{cond} = m_7h_7 - m_8h_8 \quad (21)$$

2.2.6 Coefficient of performance

Coefficient of performance was measured using three factors, which was heat absorbed by the evaporator Qevp, heat delivered from generator Qgen and pump work Wp.

$$COP = \frac{Q_{evp}}{Q_{gen} + W_p} \quad (22)$$

2.2.7 Exhaust heat calculation

The engine installed in Daewoo BH 116 was DE 12T, Diesel engine. The specification of the engine is given in Table 1. From the following equation, it can be evaluated the amount of heat available from the exhaust of the engine [34].

$$Q_{ex} = m_{eg}C_{ex}(T_1 - T_2) \quad (23)$$

Where Qex is the amount of heat available from the exhaust, Cex is the specific heat of the exhaust which is assumed to be equal to the specific heat of air at that temperature, meg is the mass flow rate of the exhaust. T1 is the exhaust initial temperature and T2 is the exhaust outlet temperature. The study was performed taking exhaust outlet temperature to be 200 °C.

m_{eg} mass flow rate of the exhaust is the sum of the mass flow rate of air that is m_a and mass flow rate of fuel that is m_f. m_{eg} was computed using the following relation.

$$m_{eg} = m_a + m_{fuel} = m_{fuel}(1+\gamma) \quad (24)$$

Where γ is the compression ratio, m_a was computed using the following relation [35].

$$m_a = \rho_o.V_{disp}.\frac{n}{60\tau} \quad (25)$$

Where ρo is the density of air Vdisp is the displacement of the engine, n is the number of revolution per minute and τ is the number of revolution of crankshaft per cycle [36].

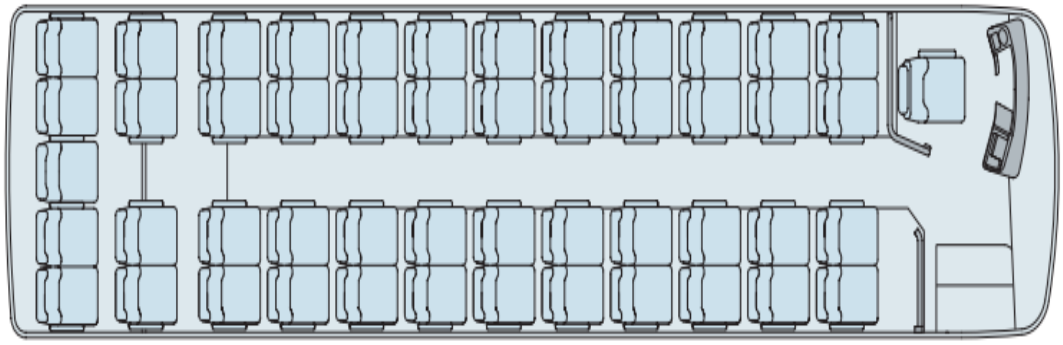

Fig. 1: Top view of BH116 bus

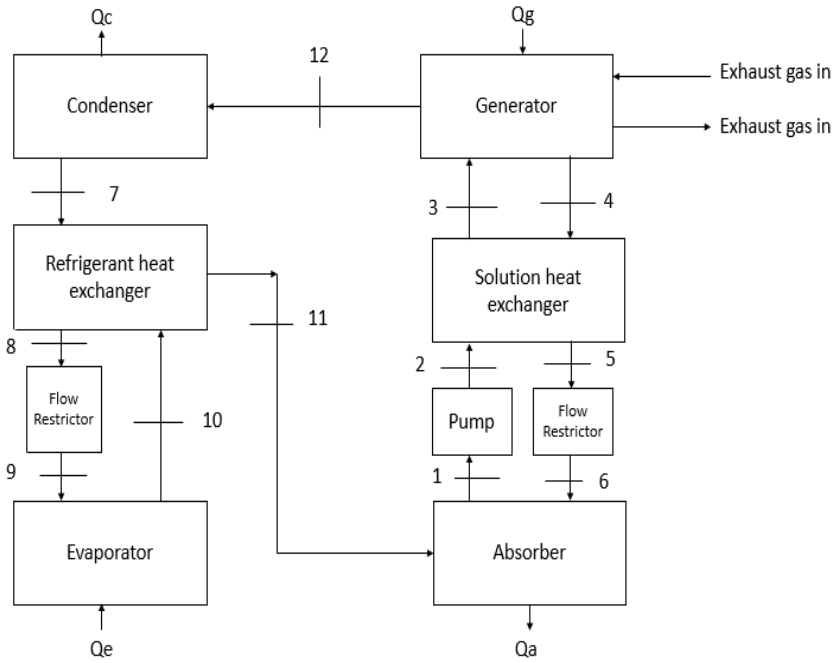

Fig. 2: Model of exhaust gas driven vapor absorption cycle

Table 1: Specifications of Daewoo BH116 engine

Model	**DE 12T, Diesel**
Type	4 cycles, water cooled
No. of cylinders	6, In-Line
Bore & Stroke	123×155 mm
Displacement	11051 cc
Maximum horsepower	300ps/2200rpm
Maximum torque	110kg.m/1300rpm
Compression ratio	17.1:1

3. Results and Discussion

3.1 Cooling load of the bus

Pakistan is amongst those countries where sun warms the surface whole year. Fig. 3 and Fig. 4 shows the variation of direct and defused radiation received from the sun on the surface in the month of June in Lahore, Pakistan.

It can be observed from Fig. 3 and Fig. 4 that the radiation starts increasing after the sunrise. The radiation increases and reaches to its peak when the sun is at zenith position and then starts decreasing until the sunset. The radiations are zero after the sunset. The data is obtained from CSP Services GmbH.

Fig. 5 shows the cooling load due to direct radiations, diffused radiations, ambient load, metabolic load, ventilation load, exhaust load, reflected load and load due to engine heat. Load due to the direct and diffused solar radiation are the main contributor in the total cooling load shown in Fig. 6.

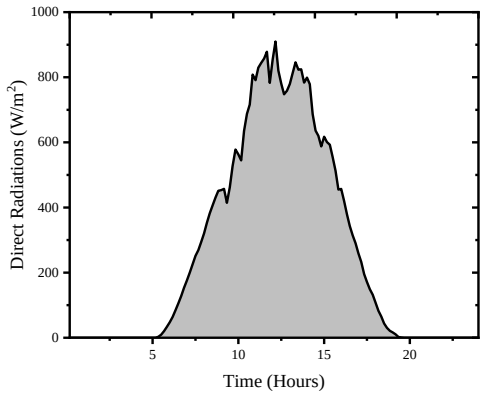

Fig. 3: Variation of direct radiation over the day

Direct and diffused radiations load varies with the variation of solar radiation intensity and solar altitude angle and it reaches to the peak when the sun is at zenith position ($\theta = 90°$).

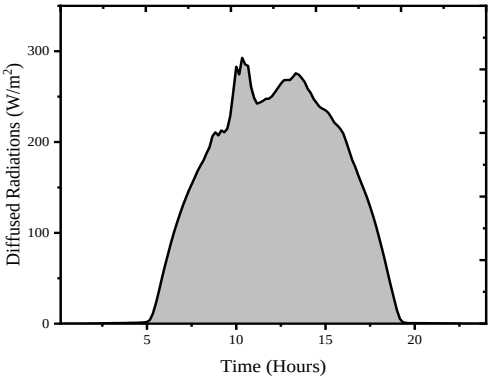

Fig. 4: Variation of diffused radiation over the span of a day in the month of June.

Direct and diffused load starts decreasing as the solar altitude angle decreases and reaches to zero at sunset. Metabolic load was calculated for 49 passengers and a driver, the metabolic rate for passenger is taken 55 W/m2 and for driver it is taken 85 W/m2 (American Society of Heating, 1961).The heat gain due to metabolic load remains constant because of no change in the number of passengers. Ventilation load was calculated measuring a constant minimum mass flow rate for cabin ventilation. A constant mass flow rate of ventilation air and a constant cabin temperature results in a constant ventilation load inside the cabin. Ambient load was measured taking a constant vehicle speed which resulted in a constant value. Cooling load due to reflection, exhaust gas and engine heat are negligible and they were assumed to be zero. Khayyam et al. [37] concluded that in a properly insulated vehicles the cooling load due to engine heat and exhaust gas can be neglected.

Fig. 6 shows the total cooling load obtained after the summation of individual cooling loads. It can be observed from Fig. 6 that the cooling load varies along the time and reaches the maximum value of 29548 W between 12 PM to 2 PM. The cooling load increases along the sun rise as the load due to direct and diffused radiation start increasing and reaches to its peak when the sun altitude angle θ is equal to 90° and then the cooling load decreases with the decrease of solar altitude angle. After the sunset the cooling load drops to the minimum value of 9903W as the load due to solar radiation is zero after the sunset. After the sunset metabolic load, ventilation load and ambient load become the main constituent of total cooling load.

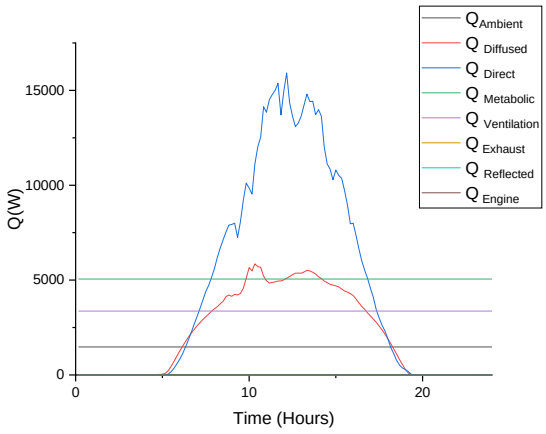

Fig. 5: Variation of individual load over the span of a day

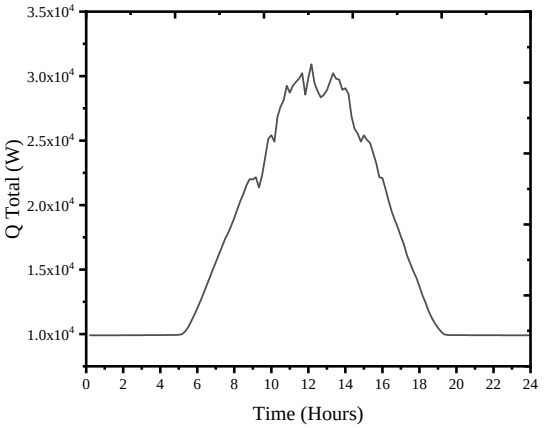

Fig. 6: Total cooling load calculation over the span of the day

3.2 Vapor absorption system Results

The computations to check the performance waste heat driven vapor absorption cycle has done using MATLAB Software platform. Fig. 2 shows the Model of exhaust gas driven vapor absorption cycle. Summary of working parameters are given in Table 2.

From Fig. 7 shows the variation of mass flow rate of the exhaust gas and exhaust heat along the engine rpm. it can be observed that as the engine rpm increases, the engine intake air increases due to which mass flowrate of exhaust gas increases. With that increased amount of intake air the fuel intake increases to keep the air fuel ratio constant, due to increased rate of burning of air fuel mixture the temperature of exhaust gas rises and with that elevateed temperature of the exhaust gas the exhaust heat also rises. When the engine is at its idling condition, the exhaust heat become insufficient to run VAC, at this condition an auxiliary system is required which produces sufficient cooling when the engine rpm are low.

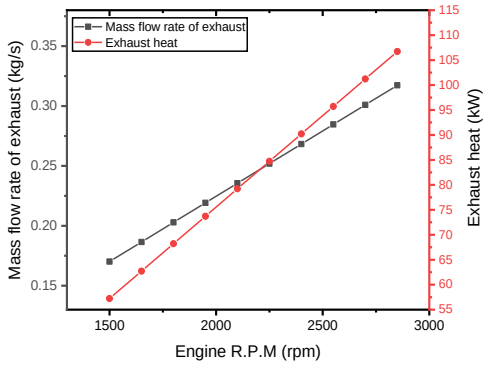

Fig. 7: Variation of exhaust mass flow rate and exhaust heat with Engine rpm

Fig. 8 shows the effect of ambient temperature on the mass flow rate of exhaust gas with the variation of engine rpm. At 25° ambient temperature, the density of air is greater as compared to 30° and 40° ambient temperature and hence the mass of intake air in the engine cylinders is higher as compared to higher ambient temperature at given engine speed. The results depict that on a warmer day the density of the ambient air decreases which results in low exhaust mass flow rate.

Fig. 9 shows the amount of cooling produced with the variation of engine rpm. As the exhaust gas increases with the increase of engine rpm, the heat availability at the generator also increases which results in an increase of amount of cooling produced at the evaporator section. It can be observed from the Fig. 9 that the peak required cooling achieved when the engine is running at 2200rpm.

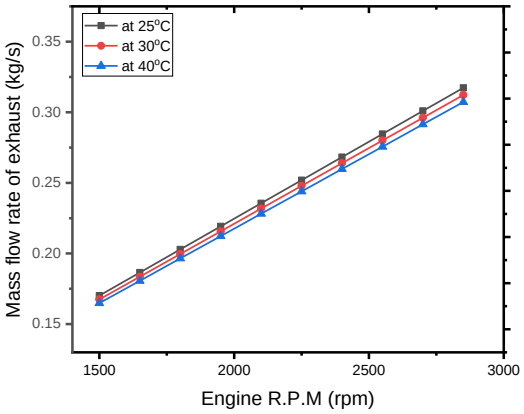

Fig. 8: FMass flow rate of Exhaust at different ambient temperature with the variation of engine rpm

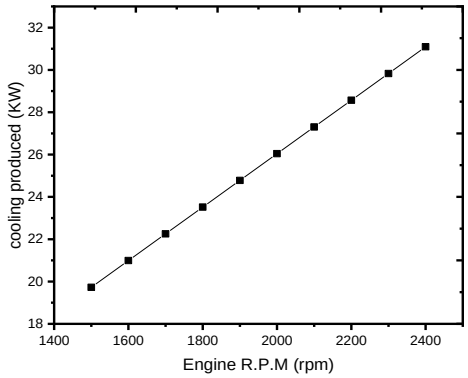

Fig. 9: Cooling produced with the variation of engine rpm

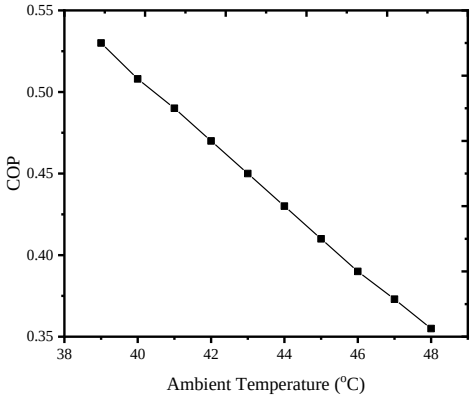

Fig. 10: Variation of COP with the variation of ambient temperature

Fig. 10 shows the variation of COP of the system with the ambient temperature. A lower

ambient temperature allows better heat rejection from condenser and absorber, which results in an increase of overall cooling capacity of the system. As the ambient temperature increase the heat transfer to the environment decreases due to which the enthalpy is high at the entry of evaporator and results in a lower COP.

Fig. 11 shows the amount of cooling produced and variation of generator heat with the variation of exhaust temperature. It can be observed from the graph that as the temperature of the exhaust increases, the generator heat increases as both are coupled together, as the generator heat increases the cooling produced also increases.

Fig. 12 shows a relation between evaporator temperature and COP of the system. It can be observed from the Fig. 12 that a higher evaporator temperature results in higher COP. With the rise of evaporator temperature, the values of refrigerant enthalpy increase and the difference between the condenser and evaporator temperature decreases which results in an increase of COP of the system.

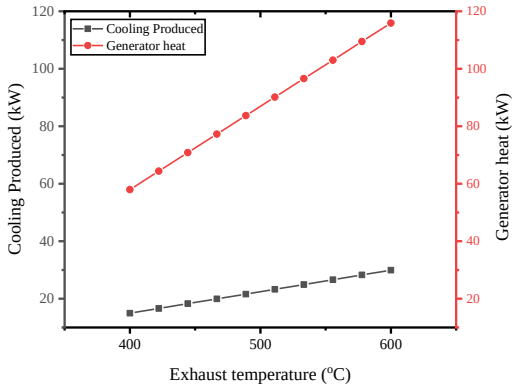

Fig. 11: Cooling produced and Generator heat with the variation of exhaust temperature

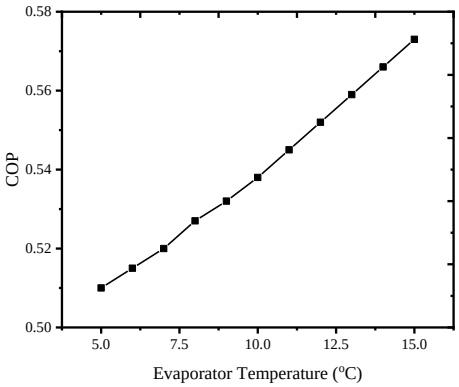

Fig. 12: Variation of COP with the variation of evaporator temperature

Fig. 13 shows that with the increase of generator temperature the COP of the system decreases. With the increase of generator temperature, the demand for heat transfer at the condenser also increases due to which the difference between condenser temperature and the set evaporator temperature increase which ultimately drops the COP of the system.

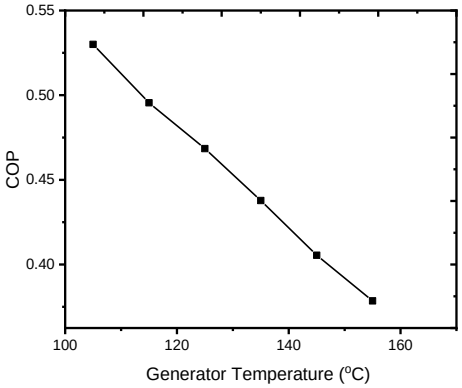

Fig. 13: Variation of COP with the variation of generator temperature

Table 2: Summary of working parameters of vapor absorption cycle

Point	Enthalpy kJ/kg	Mass flow Kg/s	Pressure kPa	Temperature ˚C	Mass fraction (x)
1	-56	0.343	369.1	40	0.421
2	-30	0.343	720.5	41.5	0.421
3	230	0.343	720.5	78	0.421
4	393	0.315	720.5	100	0.332
5	375	0.315	720.5	72	0.332
6	340	0.315	369.1	45	0.332
7	80	0.0277	720.5	40	0.998≈1
8	54	0.0277	720.5	35	0.998≈1
9	92	0.0277	369.1	5	0.998≈1
10	1290	0.0277	369.1	6	0.998≈1
11	1345	0.0277	369.1	10	0.998≈1
12	1870	0.0286	720.5	100	0.998≈1

4. Conclusion

A thermodynamic model has been developed in this work to recover waste heat from the engine exhaust of Daewoo bus BH116 to run vapor absorption cycle. The waste heat powered system is observed under Lahore weather. Parametric analysis has been performed and the operating conditions of the system are optimized. The thermodynamic model has been evaluated at various operating condition by varying the temperature of evaporator, generator and ambient temperatures. The results showed that exhaust heat driven vapor absorption cycle meets the demand of cooling requirement of the bus and achieves peak cooling demand of 29.886 KW at an engine rpm of 2250rpm. The study also showed that ambient temperature, evaporator temperature and generator temperature influence cycle performance. It has been observed that COP of the cycle increases with the increase in evaporator temperature and decreases with the increase in ambient and generator temperature. At low engine rpm the system becomes inefficient to produce required amount of cooling during peak cooling demand hours. This phenomenon can be observed during engine idling. In that case, there must be an auxiliary system installed which supply cooling during engine idling condition.

5. References

[1] Aleixo, A., Morais, S., Cabezas-gómez, L., & Ricardo, J. (2010). Using engine exhaust gas as energy source for an absorption refrigeration system. *Applied Energy*, *87*(4), 1141–1148. https://doi.org/10.1016/j.apenergy.2009.07.018.

[2] Zhang, X., Craft, E., & Zhang, K. (2017). Characterizing spatial variability of air pollution from vehicle traffic around the Houston Ship Channel area. *Atmospheric Environment*. https://doi.org/10.1016/j.atmosenv.2017.04.032.

[3] Ziyadi, M., Ozer, H., Kang, S., & Al-qadi, I. L. (2017). Vehicle Energy Consumption and an Environmental Impact Calculation Model for the Transportation Infrastructure Systems. *Journal of Cleaner Production*. https://doi.org/10.1016/j.jclepro.2017.10.292.

[4] Goyal, A., Staedter, M. A., Hoysall, D. C., Ponkala, M. J., & Garimella, S. (2017). Experimental evaluation of a small-capacity, waste-heat driven ammonia-water absorption chiller Évaluation expérimentale d ' un refroidisseur à absorption à ammoniac-eau de faible puissance alimenté par de la chaleur perdue. *International Journal of Refrigeration*, *79*, 89–100. https://doi.org/10.1016/j.ijrefrig.2017.04.006.

[5] Yuan, H., Zhang, J., Huang, X., & Mei, N. (2018). Experimental investigation on binary ammonia – water and ternary ammonia – water – lithium bromide mixture-based absorption refrigeration systems for fi shing ships. *Energy Conversion and Management*, *166* (September 2017), 13–22. https://doi.org/10.1016/j.enconman.2018.04.013.

[6] Ouadha, A., & El-gotni, Y. (2013). Integration of an ammonia-water absorption refrigeration system with a marine Diesel engine : A thermodynamic study. *Procedia - Procedia Computer Science*, *19*(Seit), 754–761. https://doi.org/10.1016/j.procs.2013.06.099.

[7] Rêgo, A. T., Hanriot, S. M., Oliveira, A. F., Brito, P., & Rêgo, T. F. U. (2014). Automotive exhaust gas flow control for an ammonia-water absorption refrigeration system. *Applied Thermal Engineering*, *64*(1–2), 101–107. https://doi.org/10.1016/j.applthermaleng.2013.12.018.

[8] Asadi, J., Amani, P., Amani, M., Kasaeian, A., & Bahiraei, M. (2018). Thermo-economic analysis and multi-objective optimization of absorption cooling system driven by various solar collectors. *Energy Conversion and Management*, *173*(February), 715–727. https://doi.org/10.1016/j.enconman.2018.08.013.

[9] Shiue, A. (2018). Original article E ff ect of operating variables on performance of an absorption chiller driven by heat from municipal solid waste incineration. *Sustainable Energy Technologies and Assessments*, *27*(1), 134–140. https://doi.org/10.1016/j.seta.2018.04.008.

[10] Buonomano, A., Calise, F., & Palombo, A. (2017). Solar heating and cooling systems by absorption and adsorption chillers driven by stationary and concentrating photovoltaic / thermal solar collectors : Modelling and

simulation. *Renewable and Sustainable Energy Reviews*, 1. https://doi.org/10.1016/j.rser.2017.10.059.

[11] Shi, Y., Li, F., Hong, D., Wang, Q., & Chen, G. (2018). Experimental study of a new ejector-absorption refrigeration cycle driven by multi-heat sources. *Applied Thermal Engineering*. https://doi.org/10.1016/j.applthermaleng.2018.01.073.

[12] Staedter, M. A., & Garimella, S. (2018a). Development of a Micro-Scale Heat Exchanger Based, Residential Capacity Ammonia-Water Absorption Chiller. *International Journal of Refrigeration*. https://doi.org/10.1016/j.ijrefrig.2018.02.016.

[13] Staedter, M. A., & Garimella, S. (2018b). International Journal of Heat and Mass Transfer Direct-coupled desorption for small capacity ammonia-water absorption systems. *International Journal of Heat and Mass Transfer*, *127*, 196–205. https://doi.org/10.1016/j.ijheatmasstransfer.2018.06.118.

[14] Wang, M., Becker, T. M., Schouten, B. A., Vlugt, T. J. H., & Ferreira, C. A. I. (2018). Ammonia / ionic liquid based double-e ff ect vapor absorption refrigeration cycles driven by waste heat for cooling in fi shing vessels. *Energy Conversion and Management*, *174* (December 2017), 824–843. https://doi.org/10.1016/j.enconman.2018.08.060.

[15] Yousfi, M. L., Saighi, M., Dalibard, A., & Eicker, U. (2017). Performance of a 5 kW hot water driven diffusion absorption Chiller. *Applied Thermal Engineering*. https://doi.org/10.1016/j.applthermaleng.2017.08.035.

[16] Aly, W. I. A., Abdo, M., Bedair, G., & Hassaneen, A. E. (2016). Development and experimental study of an ammonia water absorption refrigeration prototype driven by diesel engine exhaust heat. *Applied Thermal Engineering*. https://doi.org/10.1016/j.applthermaleng.2016.12.019.

[17] Du, S., Wang, R. Z., Chen, X., Wang, R. Z., & Chen, X. (2017). Development and experimental study of an ammonia water absorption refrigeration prototype driven by diesel engine exhaust heat. https://doi.org/10.1016/j.energy.2017.05.006.

[18] Ibrahim, N. I., Al-sulaiman, F. A., & Nasir, F. (2017). Performance characteristics of a solar driven lithium bromide-water absorption chiller integrated with absorption energy storage. *Energy Conversion and Management*, *150*(June), 188–200. https://doi.org/10.1016/j.enconman.2017.08.015.

[19] Salmi, W., Vanttola, J., Elg, M., Kuosa, M., & Lahdelma, R. (2016). Using waste heat of ship as energy source for an absorption refrigeration system. *Applied Thermal Engineering*. https://doi.org/10.1016/j.applthermaleng.2016.12.131.

[20] Shu, G., Che, J., Tian, H., Wang, X., & Liu, P. (2016). A compressor-assisted triple-effect H2O-LiBr absorption cooling cycle coupled with a Rankine Cycle driven by high-temperature waste heat. *Applied Thermal Engineering*. https://doi.org/10.1016/j.applthermaleng.2016.08.073.

[21] Xu, Z. Y., & Wang, R. Z. (2017b). Simulation of solar cooling system based on variable effect LiBr-water absorption chiller. https://doi.org/10.1016/j.renene.2017.06.069.

[22] Xu, Z. Y., & Wang, R. Z. (2017a). Comparison of CPC driven solar absorption cooling systems with single , double and variable e ff ect absorption chillers, *158*(June), 511–519. https://doi.org/10.1016/j.solener.2017.10.014.

[23] Yang, S., Qian, Y., Wang, Y., & Yang, S. (2017). A novel cascade absorption heat transformer process using low grade waste heat and its application to coal to synthetic natural gas. *Applied Energy*, *202*, 42–52. https://doi.org/10.1016/j.apenergy.2017.04.028.

[24] Palomba, V., Aprile, M., Vasta, S., Gullì, G., Freni, A., & Motta, M. (2016). Study and evaluation of two innovative waste-heat driven refrigeration systems for fishing vessels applications. *Energy Procedia*, *101*(September), 838–845. https://doi.org/10.1016/j.egypro.2016.11.106.

[25] Mumtaz, M., Khan, A., Ibrahim, N. I., Saidur, R., Mahbubul, I. M., & Al-sulaiman, F. A. (2016). Performance assessment of a solar powered ammonia – water absorption refrigeration system with storage units. *Energy Conversion and Management*, *126*, 316–328. https://doi.org/10.1016/j.enconman.2016.08.004.

[26] Zisheng, L., & Ruzhu, W. (2016). Experimental performance study of sorption refrigerators driven by waste gases from fishing vessels diesel engine. *Applied Energy*, *174*, 224–231. https://doi.org/10.1016/j.apenergy.2016.04.102.

[27] Shi, Y., Chen, G., & Hong, D. (2015). The performance analysis of a novel absorption refrigeration cycle used for waste heat with large temperature glide. *Applied Thermal Engineering*. https://doi.org/10.1016/j.applthermaleng.2015.10.034.

[28] Wang, R. Z., Xu, Z. Y., Pan, Q. W., Du, S., & Xia, Z. Z. (2016). Solar driven air conditioning and refrigeration systems corresponding to various heating source temperatures, *169*, 846–856. https://doi.org/10.1016/j.apenergy.2016.02.049.

[29] Brückner, S., Liu, S., Miró, L., Radspieler, M., Cabeza, L. F., & Lävemann, E. (2015). Industrial waste heat recovery technologies : An economic analysis of heat transformation technologies, *151*, 157–167. https://doi.org/10.1016/j.apenergy.2015.01.147.

[30] Cao, T., Lee, H., Hwang, Y., Radermacher, R., & Chun, H. (2015). Performance investigation of engine waste heat powered absorption cycle cooling system for shipboard applications. *Applied Thermal Engineering*, *90*, 820–830. https://doi.org/10.1016/j.applthermaleng.2015.07.070.

[31] Patel, B., Desai, N. B., & Kachhwaha, S. S. (2017). Optimization of waste heat based organic Rankine cycle powered cascaded vapor compression-absorption refrigeration system. *Energy Conversion and Management*, *154* (July), 576–590. https://doi.org/10.1016/j.enconman.2017.11.045.

[32] Risk, N. C. D., & Collaboration, F. (2016). A century of trends in adult human height, 1–29. https://doi.org/10.7554/eLife.13410.

[33] Chevella, S., & Hyderabad, R. R. D. (2013). DESIGN OF AIR CONDITIONING SYSTEM, HVAC System *2*(12), 7460–7464.

[34] Kilicarslan, A., & Qatu, M. (2017). Exhaust gas analysis of an eight cylinder gasoline engine based on engine speed. *Energy Procedia*, *110*(December 2016), 459–464. https://doi.org/10.1016/j.egypro.2017.03.169.

[35] Christy, C., & Toossi, R. (2004). Adsorption Air-Conditioning for Containerships and Vehicles.

[36] Fonseca, N., Casanova, J., María, J., & Martínez, L. (2016). Methodology for instantaneous average exhaust gas mass fl ow rate measurement, *49*, 52–62. https://doi.org/10.1016/j.flowmeasinst.2016.04.007.

[37] Khayyam, H., Kouzani, A. Z., Hu, E. J., & Nahavandi, S. (2011). Coordinated energy management of vehicle air conditioning system. *Applied Thermal Engineering*, *31*(5), 750–764. https://doi.org/10.1016/j.applthermaleng.2010.10.022.